Full length article

Role of scaffold mean pore size in meniscus regeneration

Zheng-Zheng Zhang [a,1], Dong Jiang [a,1], Jian-Xun Ding [b,*], Shao-Jie Wang [a], Lei Zhang [c], Ji-Ying Zhang [a], Yan-Song Qi [a], Xue-Si Chen [b], Jia-Kuo Yu [a,*]

[a] Institute of Sports Medicine, Beijing Key Laboratory of Sports Injuries, Peking University Third Hospital, Beijing 100191, PR China
[b] Key Laboratory of Polymer Ecomaterials, Changchun Institute of Applied Chemistry, Chinese Academy of Sciences, Changchun 130022, PR China
[c] Beijing Key Laboratory of Biofabrication and Rapid Prototyping Technology, Department of Mechanical Engineering, Tsinghua University, Beijing 100084, PR China

ARTICLE INFO

ABSTRACT

Recently, meniscus tissue engineering offers a promising management for meniscus regeneration. Although rarely reported, the microarchitectures of scaffolds can deeply influence the behaviors of endogenous or exogenous stem/progenitor cells and subsequent tissue formation in meniscus tissue engineering. Herein, a series of three-dimensional (3D) poly(ε-caprolactone) (PCL) scaffolds with three distinct mean pore sizes (*i.e.*, 215, 320, and 515 μm) were fabricated *via* fused deposition modeling. The scaffold with the mean pore size of 215 μm significantly improved both the proliferation and extracellular matrix (ECM) production/deposition of mesenchymal stem cells compared to all other groups *in vitro*. Moreover, scaffolds with mean pore size of 215 μm exhibited the greatest tensile and compressive moduli in all the acellular and cellular studies. In addition, the relatively better results of fibrocartilaginous tissue formation and chondroprotection were observed in the 215 μm scaffold group after substituting the rabbit medial meniscectomy for 12 weeks. Overall, the mean pore size of 3D-printed PCL scaffold could affect cell behavior, ECM production, biomechanics, and repair effect significantly. The PCL scaffold with mean pore size of 215 μm presented superior results both *in vitro* and *in vivo*, which could be an alternative for meniscus tissue engineering.

Statement of Significance

Meniscus tissue engineering provides a promising strategy for meniscus regeneration. In this regard, the microarchitectures (*e.g.*, mean pore size) of scaffolds remarkably impact the behaviors of cells and subsequent tissue formation, which has been rarely reported. Herein, three three-dimensional poly(ε-caprolactone) scaffolds with different mean pore sizes (*i.e.*, 215, 320, and 515 μm) were fabricated *via* fused deposition modeling. The results suggested that the mean pore size significantly affected the behaviors of endogenous or exogenous stem/progenitor cells and subsequent tissue formation. This study furthers our understanding of the cell-scaffold interaction in meniscus tissue engineering, which provides unique insight into the design of meniscus scaffolds for future clinical application.

1. Introduction

Meniscus plays a crucial role in load absorption, lubrication, and maintaining stability of the knee joint. Meniscal tear is one of the most frequently recorded sports medicine injuries with mean incidence of 66/100,000 in the United States [1]. As a usual surgical option, either partial or total meniscectomy would increase the stress on articular cartilage, even leading to knee damage and osteoarthritis [2]. Various surgical attempts to repair the torn meniscus have been used but are only effective in the vascular zone and often associated with a re-rupture rate of 30% [3]. Meniscus tissue engineering, which aims to regenerate the damaged tissue, offers a potential solution strategy to facilitate traditional repair or meniscectomy [4]. However, there still remains an unmet need for optimal biomaterials with both appropriate framework and sufficient mechanical strength to support the behaviors of endogenous or exogenous stem/progenitor cells for regeneration of meniscus.

The microarchitectures of biomaterials have been shown to significantly affect the behaviors of cells both *in vitro* and *in vivo* [5,6].

---

* Corresponding authors.
  E-mail addresses: yujiakuo@126.com (J.-K. Yu), jxding@ciac.ac.cn (J.-X. Ding).
[1] Zheng-Zheng Zhang and Dong Jiang contributed equally to this work.

In particular, the mean pore size of scaffold can modulate cell-matrix interaction effectively [7,8]. It has been demonstrated that larger pores of scaffolds facilitate cell diffusion and migration, while smaller ones provide a higher surface area of scaffold for cell adhesion [9]. The subsequent cell proliferation, differentiation, and matrix deposition may contribute to the biochemical and mechanical properties of regenerated constructs [6,7]. Therefore, the understanding of mechanisms, by which scaffold architecture (*e.g.*, mean pore size) affects cell behavior and subsequent tissue formation, is a prerequisite for successful meniscus tissue engineering.

So far, few studies have investigated the optimal mean pore sizes of scaffolds for resembling tissue engineered meniscus [10,11]. As a typical example, Mandal et al. designed a multilayered silk scaffold composed of three individual layers with different pore sizes (*i.e.*, 350–400, 500–600, and 60–80 μm) and orientations. Although the implanted seed cells could migrate though the large pores and the smaller pores improved the deposition of extracellular matrix (ECM), the whole platform exhibited inferior mechanical property compared to native meniscus [11]. When generating the tissue engineered meniscus as a weight-bearing construct, attention should also be paid to the mechanical properties of the biomaterial itself, which interact with the microarchitecture [4,12].

In this context, we utilized fused deposition modeling (FDM) to fabricate a series of three-dimensional (3D) poly(ε-caprolactone) (PCL) scaffolds with three distinct mean pore sizes (*i.e.*, 215, 320, and 515 μm). The above mean pore sizes were selected based on the previously reported results that the selected ones have positive effects on tissue formation [7,12–14]. The purpose of the present research was to investigate the influences of various mean pore sizes of scaffold on (1) *in vitro* proliferation, differentiation, and matrix production and deposition of mesenchymal stem cells (MSCs), which has been widely used as the seed cells for meniscus tissue engineering; (2) *in vivo* tissue regeneration (*i.e.*, cellular infiltration, vascularization, and fibrocartilaginous tissue formation) and the chondroprotection in a rabbit model (Fig. 1). The results of present study might verify the effect of mean pore size on outcome of the 3D-printed PCL scaffold used for meniscus tissue engineering and further offer unique insight into meniscus regeneration.

2. Materials and methods

2.1. Fabrication of 3D PCL scaffolds

Medical grade PCL (number-average molecular weight (M_n) = 74,600 g mol^{-1} and melting point (MP) = 52.9 °C) was granted by Changchun SinoBiomaterials Co., Ltd. (Changchun, PR China). During the fabrication process, PCL was melted and extruded through a heated metal nozzle. The nozzle, which was controlled by computer-aided manufacturing software (Delta Tau Data Systems Inc., Chatsworth, CA, USA), could be moved both vertically and horizontally. As listed in Supplementary Table S1, the processing parameters were set to fabricate three distinct scaffolds with different mean pore sizes of 215, 320, and 515 μm, and a specification of 10 mm-diameter and 1.5 mm-thick. The surface morphologies of PCL scaffolds were observed under an S-4800 scanning electron microscope (SEM; Hitachi, Japan) operated at an acceleration voltage of 15.0 kV (Fig. S1A–C, Supplementary data). Mean pore sizes and road widths were measured with Image-Pro Plus 6.0 software (Media Cybernetics, Silver Spring, MD, USA; Supplementary Fig. S1D–I). Porosities were determined according to the previous reported approach [15]. The detail operation and equation were shown in Supplementary data.

2.2. Characterization of PCL scaffolds with various mean pore sizes

The surface wettability of all scaffolds was determined by measuring water contact angle (WCA) using the sessile drop method according to the previously reported protocol [16]. The degradation properties of scaffolds were assessed using mass loss ratio and water absorption ratio. The above values were calculated as shown in Supplementary data.

The surface area per unit volume (SA/V) was estimated using a previously described Eq. (1) [9]. It means a sufficiently high specific surface provided for a critical number of cells attached to the scaffold [7].

$$SA/V = \frac{3.65}{l} \times \sqrt{\frac{\rho^*}{\rho_s}} \tag{1}$$

In Eq. (1), l is the edge length of tetrakaidecahedron, ρ^* is the density of PCL scaffold, and ρ_s is the density of raw PCL. Zein et al. have demonstrated that FDM process did not result in a significant change of PCL molecular weight and crystallinity fraction [17], the relative density (*i.e.*, ρ^*/ρ_s) of PCL scaffold is 1. Based on the previous assumption that the pore diameter can be calculated from the edge length by $d = 2.78l$ [9], we calculated that SA/V of PCL scaffold used in this study is inversely related to the mean pore size (*i.e.*, d) by Eq. (2).

$$SA/V = \frac{10.15}{d} \tag{2}$$

2.3. Harvest, culture, and implantation of MSCs

All experimental protocols of animals were approved by the local Institutional Animal Care and Use Committee complied with the "Guide for the Care and Use of Laboratory Animals" published by the National Academy Press (NIH Publication No. 85-23, revised 1996). Bone marrow-derived MSCs were isolated from 3-month-old New Zealand White rabbits with average weight of approximately 3.0 kg. Isolation, cultivation, and tri-lineage differentiation potential assays of MSCs were performed according to a previously described protocol [18]. The tri-lineage differentiation potential results of MSCs were shown in Supplementary data. MSCs were seeded between the second and third passage using centrifugal method [19]. Briefly, the scaffold was placed at the bottom of 1.5 mL centrifugal tube, and 50.0 μL of concentrated cell solution (2.5×10^5 cells/scaffold) was added. The tube was centrifuged at 500 rpm for 1 min and then turned over as one loop. The process was repeated three consecutive times. For *in vitro* differentiation, the scaffolds were cultured under chemically defined Dulbecco's modified Eagle's medium (DMEM supplemented with 0.1 μM dexamethasone, 50.0 μg mL^{-1} ascorbate 2-phosphate, 40.0 μg mL^{-1} L-proline, 100.0 μg mL^{-1} sodium pyruvate, and its supplements (6.25 μg mL^{-1} insulin, 6.25 μg mL^{-1} transferrin, and 6.25 ng mL^{-1} selenous acid) with 10 ng mL^{-1} transforming growth factor-β3 (TGF-β3); Cyagen Biosciences Inc., Santa Clara, CA, USA).

2.4. Initial cell adhesion assessment

The initial cell adhesion in the scaffolds with different mean pore sizes was determined by initial adhesion number [16]. Briefly, MSCs seeded on different scaffolds were incubated for 1, 3, 5, or 7 h. At each time point, the cell-loaded scaffolds were washed with phosphate-buffered saline (PBS) and then incubated in 0.25% (W/V) trypsin-EDTA (EDTA, ethylenediaminetetraacetic acid; Gibco BRL Co. Ltd., Gaithersburg, MD, USA) for 10 min to detach cells from the scaffolds. Cell number was detected using an automated cell counter (Scepter™, Merck Millipore Co., USA).
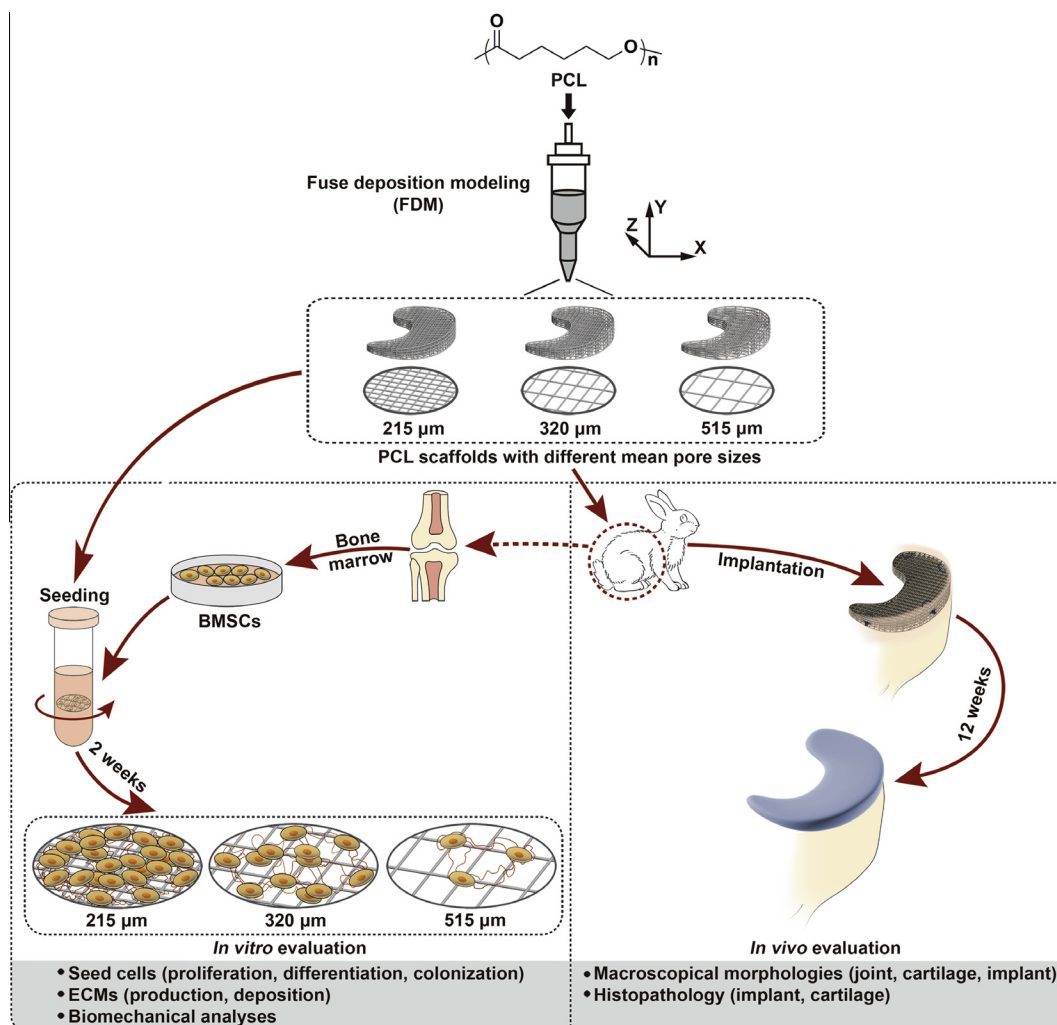
Fig. 1. Schematic illustration for regeneration of tissue engineered meniscus. *In vitro* and *in vivo* evaluation of PCL scaffolds with different mean pore sizes.

2.5. Cell viability and proliferation measurement

The viabilities of cells in the scaffolds with different mean pore sizes were evaluated with a LIVE/DEAD viability/cytotoxicity kit assay (Invitrogen, Carlsbad, CA, USA) after 24 h culture as described previously [19]. LeicaTCS-SP 5 confocal microscopy (Leica, Nussloch, Germany) was used for image capture. The numbers of live and dead cells were quantified, and then the percentage of live cells was calculated using Image-Pro Plus software. To investigate the effects of various mean pore sizes on cell proliferation, the metabolic activity of cells was determined using a Cell Counting Kit-8 (CCK-8) assay (Dojindo Laboratories, Kamimashiki Gun, Kumamoto, Japan) according to the manufacture protocol.

2.6. Biochemical assessment

The samples were digested in a pre-prepared papain solution (containing 0.5 M EDTA, 0.05 M cysteine hydrochloride, and 1 mg mL^{-1} papain enzyme) (Sigma, St. Louis, MO, USA) at 60 °C overnight. The contents of deoxyribonucleic acid (DNA), glycosaminoglycans (GAG), and type I and type II collagen (Col I and Col II) were determined using fluorometry [16], 1,9-dimethylmethylene blue (DMMB) dye-binding assay [20], and enzyme-linked immunosorbent assay (ELISA) kit (Chondrex Inc.,

WA, USA) [21], respectively. The detail operation protocol was shown in Supplementary data.

2.7. Gene expression analyses

Real-time reverse transcription polymerase chain reaction (RT-PCR) was performed to determine gene expression. The fibrochondrogenesis (Col II, aggrecan (AGC), and Col I), osteogenesis (alkaline phosphatase (ALP) and hypertrophy (Col X)), and adhesion gene markers (integrin β1 (ITGB1)) were assessed. The procedure and the PCR primers were shown in Supplementary data.

2.8. Immunofluorescence staining

After culture for two weeks, the deposition of Col I and Col II was visualized through immunofluorescence. The detail operation protocol was shown in Supplementary data. The cytoskeleton of cells in the scaffolds was also stained with rhodamine phalloidin (100.0 nM; Cytoskeleton Inc., Denver, CO, USA), and then the samples were observed by confocal laser scanning microscopy (CLSM; Leica TCS-SP8, Leica Microsystems, Nussloch, Germany).

By using Imaris software (Version 7.4.2; Bitplane, Zurich, Switzerland), the volume data were used to create 3D renderings of the seeded scaffolds, thus the areas of MSC colonization and Col II deposition could be quantitatively assessed. The capture of

3D structure and area measurement were performed using a previous reported protocol [19]. Briefly, the 3D structure graphs were reconstructed using Imaris software, and then the areas-creation algorithm was utilized to locate MSC colonization (green fluorescence in LIVE/DEAD images) and Col II deposition (red fluorescence in Col II immunofluorescence images). The voxel intensity data were exchanged to area coordinate data to quantitatively analyze the areas of MSC colonization and Col II deposition.

2.9. Biomechanical analyses

The biomechanical properties of specimens were assessed using a material testing machine (AG-IS, Shimadzu, Japan) [22]. For tensile modulus, the rectangular-shaped specimens of 1.5 mm thick were cut from the samples, which were tested to ultimate failure at a rate of 0.5 mm min^{-1} [23]. For compressive modulus, the cylindrical disks of 6 mm diameter and 1.5 mm thickness were cut using trephine from the constructs [24]. Subsequently, the samples were compressed at a constant stress rate of 0.1 mm min^{-1}. The elastic modulus was analyzed from the linear portion of stress-strain curve [25]. The tensile and compressive moduli were also detected on cell-loaded constructs after 28 days of culture to investigate whether the synthesized ECM would have an influence on the biomechanical properties of scaffolds.

2.10. Animal surgery procedure

Twenty-four New Zealand white rabbits weighing 3.0 kg (3 months-old, $n = 6$ for each group) were used for animal experiments. The implantation procedure was performed according to a previously described proposal [26]. Briefly, after anesthesia and routine preparation, the right knee was approached through a medial parapatellar incision. A total meniscectomy was performed by resecting medial meniscus sharply along the periphery and detached from its anterior and posterior junction without injuring the medial collateral ligament. The acellular scaffold was shaped into semilunar disk using the removed meniscus as a template and then sutured to the adjacent synovium and ligamentous structures with nonresorbable No. 4-0 suture (Ethicon, Somerville, NJ, USA). The joint capsule, subcutaneous tissue, and skin were closed with No. 3-0 Vicryl suture (Ethicon). Only total resection of the medial meniscus in right knee was performed as Meni group ($n = 6$), while the left knee with sham operation involving exposure of the medial joint and closure in layers was considered as a positive control ($n = 6$). After the operation, the animals were allowed unlimited movement. The antibiotic prophylaxis was continued for 3 days. Six rabbits of each group were killed with pentobarbital sodium at week 12 after the operation.

2.11. Evaluation of joints and menisci

Knee joints were excised, and then the tibial surface with the implants in place and the exposed femoral condyles were photographed. The joints and menisci were grossly evaluated by Gross Assessment of Joint Changes Score [27] and Gross Evaluation of Meniscus Implant Score [28], respectively. Then the implant was dissected from the tibia. The osteochondral specimens and explants were fixed in 10% (V/V) neutral buffered formalin (Sigma Diagnostics, St. Louis, MO, USA) and decalcified in 10% ethylenediaminetetraacetic acid (Titriplex® III, Merck, Darmstadt, Germany) for 3 weeks. The osteochondral specimens were sectioned in the axial plane at the midpoint of the medial femoral condyle and in the coronal plane at the midpoint of the tibial plateau as described previously [26]. The implants were cut to produce blocks allowing histological sections that showed outer and inner regions, and superior and inferior surfaces of the regenerated menisci. The

samples were then dehydrated and embedded in paraffin. Serial 6-μm thick sections were cut and stained with hematoxylin and eosin (H&E), toluidine blue (TB, as a label for proteoglycans), and picric-sirius red (PSR, i.e., staining for distinguishing Col I and Col III). In addition, sections of explants were treated by an immunohistochemistry procedure with labeling of Col I and Col II (Calbiochem, Novabiochem, Boston, MA, USA). The sections were analyzed blindly according to the meniscus histology scoring system [28]. Moreover, immunohistochemical analyses were employed to study the differences of collagen contents within the implants. Integrated optical density (IOD) value of each microimage was measured with Image-Pro Plus 6.0 software, which was used for semiquantitative analyses.

2.12. Evaluation of joints cartilages

For assessments of chondroprotective effects of the scaffolds, the cartilages of femur and tibia were macroscopically evaluated blindly according to the criteria of the International Cartilage Repair Society (ICRS) cartilage lesion classification [29]. In addition, slides of femur and tibia were stained with H&E and TB, and graded blindly according to Mankin grading system [30].

2.13. Statistical analyses

All statistical data were expressed as mean ± standard deviation (SD)/standard error of mean (SEM). All experiments were repeated at least three times. Significances of the results were analyzed with ANOVA test and repeated measure tests with Bonferroni correction. All datum analyses were performed using SPSS statistical software (Version 15.0; SPSS Inc., Chicago, IL, USA). $P < 0.05$ was considered statistically significant, and $P < 0.01$ and $P < 0.001$ were considered highly significant.

3. Results

3.1. Effect of scaffold mean pore size on specific surface area

As summarized in Table 1 and Supplementary Fig. S2, no significant difference in surface wettability and degradation ratio was found in all three PCL scaffolds ($P > 0.05$). Moreover, their specific surface areas were also investigated by SA/V, which means a sufficiently high specific surface provided for a critical number of cells attached to the scaffold [7,31]. As was consistent with the previous work [9], the SA/V was inversely proportional to the mean pore diameter (d) according to Eq. (2).

3.2. Effect of scaffold mean pore size on initial cell attachment, viability, and proliferation

A growing tendency was found with cell adhesion in all three groups during the culture period of 1–7 h (Fig. S3A, Supplementary data). The cells attached on both the 215 and 320 μm scaffolds were more than those on the 515 μm scaffold at each time point. These results indicated the effect of pore architecture on the initial cell attachment.

In terms of cell viability, the scaffolds with various mean pore sizes were confirmed to support cell activity (Fig. S3C, Supplementary data), and the 320 μm scaffold sustained the greatest percentage of live cells in all three groups (Fig. S3B, Supplementary data). Lots of dead cells were detected in the scaffold with pore size of 215 μm, which might be explained by inadequate nutrient supply to the interior of the smallest pore within 24 h.

In CCK-8 assay, the MSCs in all the three groups showed an increasing proliferative tendency during the culture period

Table 1
Summary of different FDM conditions used to alter parameters of PCL scaffolds.

Code		215 μm	320 μm	515 μm
Pore size (μm)		215 ± 23	320 ± 25	515 ± 21
Road width (μm) [17]		304 ± 21	315 ± 10	328 ± 15
Space (μm)		200	300	500
Porosity (%)		61.5	63.1	64.2
SA/V (μm^{-1})		0.0472	0.0317	0.0197
WCA (°)		78.3 ± 2.0	77.2 ± 8.1	76.5 ± 7.0
Mass loss (%)	4th week	0.92 ± 0.06	0.93 ± 0.05	0.95 ± 0.04
	8th week	1.0 ± 0.09	0.98 ± 0.03	1.0 ± 0.05
	12th week	1.1 ± 0.02	1.1 ± 0.08	1.1 ± 0.03
Water absorption (%)	4th week	8.5 ± 0.3	8.7 ± 0.3	8.8 ± 0.5
	8th week	9.0 ± 0.5	9.1 ± 0.5	9.1 ± 0.4
	12th week	9.5 ± 0.2	9.4 ± 0.6	9.3 ± 0.7

(Fig. S3D, Supplementary data). Consistent with the above data, the optical density (OD) values in the 515 μm scaffold group were significantly lower than those in the other groups. Although the mean pore size had different effects on the survival of seeded cells in the 215 and 320 μm scaffolds for 24 h (Fig. S3B, Supplementary data), they did not affect the proliferation of MSCs after 7 days in culture. Similar to the cell proliferation assay, the 515 μm scaffold group was also shown the lowest cell number compared with the other two groups through DNA content assays (Fig. S3E, Supplementary data).

3.3. Effect of scaffold mean pore size on MSC gene expression and synthesis of ECM

The GAG and collagen contents were used as a criterion of fibrocartilaginous matrix production by MSCs in differentiation culture. The GAG content in all three groups showed an increasing tendency during culture for 14 days. On day 7, there was approximate 5-fold higher GAG content in the 215 and 320 μm scaffold groups than that in the 515 μm scaffold group (Fig. S4A). By day 14, there were still significantly higher GAG contents in the former two groups than that in the 515 μm scaffold group. According to ELISA assay of the syntheses of Col I and Col II in these constructs, the scaffolds with mean pore sizes of 215 and 320 μm also produced significantly more Col II than the 515 μm scaffold after 14-day culture (Fig. S4C, Supplementary data). However, there was a relatively less Col I contrast to Col II after 2 weeks culture *in vitro*, and no significant difference of Col I production was shown in various pore size groups (Fig. S4B, Supplementary data).

In support of the ECM production assays, the increased expression of fibrochondrogenesis-specific genes (*i.e.*, Col II and AGC) was observed in all three groups after a 2-week culture. However, higher gene expression levels exhibited in the scaffolds with mean pore sizes of 215 and 320 μm compared with those of 515 μm scaffold group in 2-week culture (Fig. S4D, Supplementary data). Col I gene expression was still relatively low and not significantly changed during *in vitro* culture. This might be due to that the chemically defined medium mainly induced chondrogenic differentiation of MSCs with more Col II and AGC gene expression. Moreover, there were no significant change in the expression of hypertrophic marker (Col X) and osteogenic gene (ALP) in all three groups (*P* > 0.05). No significant change was found with the expression of an adhesion marker (*i.e.*, ITGB1) between those on day 7 and 14 in all three groups (*P* > 0.05), which suggested that the physicochemical parameters of PCL scaffolds might not influence the behaviors of seed cells. The above results indicated the importance of the microarchitectures, especially mean pore size, on the MSC fibrochondrogenesis gene expression and the synthesis of ECM.

The microimage of Col II immunofluorescence was matched with the result of ELISA assay and relative mRNA expression. The synthesized Col II was presented in all three groups after 14 days of culture (Fig. S5, Supplementary data). The scaffold with the largest mean pore size of 515 μm had the lowest content of Col II in comparison to the scaffolds with mean pore size of 215 and 320 μm. However, little Col I was synthesized in all three groups and almost undetectable (data not shown).

3.4. Effect of scaffold mean pore size on MSC colonization and Col II deposition

According to the results of quantitative assessment, the surface area covered by live MSCs on the 215 μm scaffold was 1.6 times higher than that of the 320 μm scaffold group and 3.58 times higher than that on the 515 μm scaffold (*P* < 0.05; Fig. 2A–C). Moreover, in cytoskeleton immunostaining microimages, MSCs seeded on the 215 μm scaffold showed 3D colonization and bridged neighboring fibers, while those on the 515 μm scaffold were isolated (Fig. 2D and F). In terms of the Col II deposition, a larger area of synthesized matrix around the pore in the 215 μm scaffold was shown than those in the other two groups (*P* < 0.05; Fig. 2G–I). In addition, there was a strong linear relationship between SA/V, and the areas of MSC colonization and Col II deposition (*P* < 0.05; Fig. 2J–K). These results indicated the effect of the scaffold mean pore size on MSC colonization and Col II deposition, and a greater value was found with the 215 μm scaffold group.

3.5. Effect of mean pore size on scaffold biomechanical properties

Before cell seeding, the tensile modulus of the scaffold with a mean pore size of 215 μm was 32.49 MPa, which was significantly higher than those of the other two groups (320 μm: 11.33 MPa, 515 μm: 5.99 MPa). Similarly, greater compressive modulus of the 215 μm scaffold group (20.42 MPa) was shown compared to those of the other two groups (320 μm: 9.31 MPa, 500 μm: 3.48 MPa). After 28 days culture *in vitro*, with the effect of synthesized matrix, the tensile and compressive moduli of all groups were increased, with significance in the compressive moduli of 320 μm scaffold group (*P* < 0.01; Fig. 3).

3.6. Evaluation of joint and meniscus implant

All the rabbits restored normal gait patterns in 2 weeks postoperatively. No complications and significant weight change were seen. There were no sign of inflammation and swelling in the joint, and the synovial fluid was clear postmortem. The macroscopic observation of the operated joints was showed in Fig. 4, and the joint gross assessment results were summarized in Fig. 5 and Supplementary Table S2. In the positive control group, the meniscus was intact in the control knee joint with no sign of degradation, while various degrees of cartilage damage were observed in the other operated joints. Specially, significantly lower joint degeneration was observed in the 215 μm scaffold group when compared to those of the other groups (*P* < 0.05; Fig. 5A).

After 12 weeks of transplantation, all the scaffolds formed meniscus-like tissue *in vivo* (Fig. 4iii, vi, and ix). The surface of 215 μm scaffold became smoother and better integrated to the joint with no sign of disruption or gap formation. This neomeniscus maintained the original scaffold shape and size approximately, while it was slightly larger than the origin construct. The shape and size of original scaffold with mean pore size of 320 μm was observed obviously collapse, especially in the posterior horn. The shape of 515 μm scaffold was also obviously deformed. Moreover, some of them were not discontinuous and distinguishable. The gross evaluation scores were shown in Supplementary Table S3.
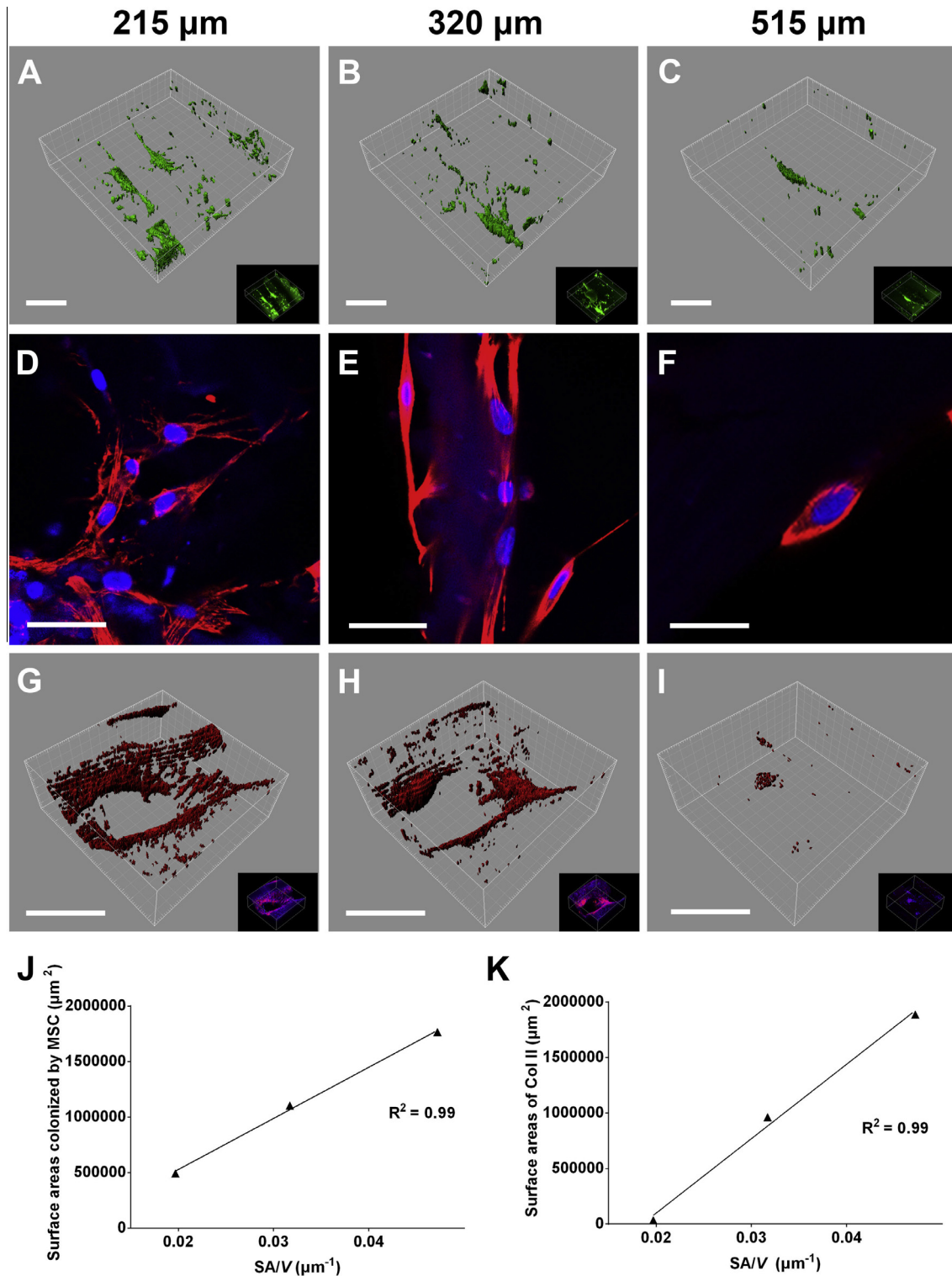
Fig. 2. Effect of scaffold mean pore size on MSC colonization and Col II deposition. Representative 3D microimages of MSC colonization and Col II deposition in scaffolds with various mean pore sizes (A–C). The surface area covered by live MSCs was the greatest on the 215 μm scaffold in all three groups. Green fluorescence marked live MSCs. Scale bar represented 300 μm. MSCs colonized and bridged neighboring fibers in the former group, while those placed on the latter were isolated (D–F). Red fluorescence dyed cytoskeleton, and blue fluorescence stained nuclei. Scale bar represented 50 μm. The largest areas of synthesized matrices around the pores were shown in the 215 μm scaffold compared with the other two scaffolds (G–I). Red fluorescence marked Col II. Scale bar represented 300 μm. Effect of specific surface area on areas of MSC colonization (J) or Col II deposition (K) in scaffolds with various mean pore sizes ($n = 3$; $R^2 = 0.99$, $P < 0.05$). (For interpretation of the references to colour in this figure legend, the reader is referred to the web version of this article.)

There were significant differences in total scores ($P < 0.05$; Fig. 5B), and better results in implant integration and tear were shown with the 215 μm scaffold ($P < 0.05$).

According to the histopathological evaluation of implants (Figs. 6–9; Supplementary Table S4), there was no significant inflammatory cell infiltration in the implants. The foreign body
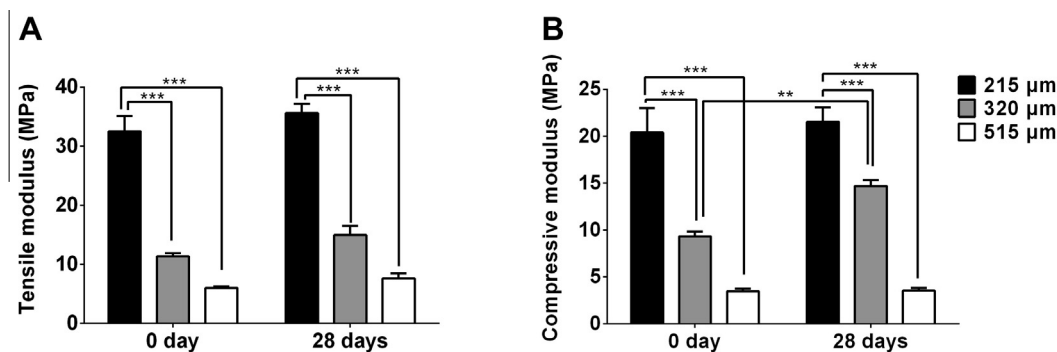
Fig. 3. Biomechanical properties. Tensile modulus of 215 μm scaffold was the highest in all three groups before and after 28-day culture (A; $n = 3$; $***P < 0.001$). The compressive modulus of 215 μm scaffold also showed the greatest values (B; $n = 3$; $***P < 0.001$). Moreover, there was a significant increase in compressive modulus in the 320 μm scaffold group after *in vitro* culture ($n = 3$; $**P < 0.01$).
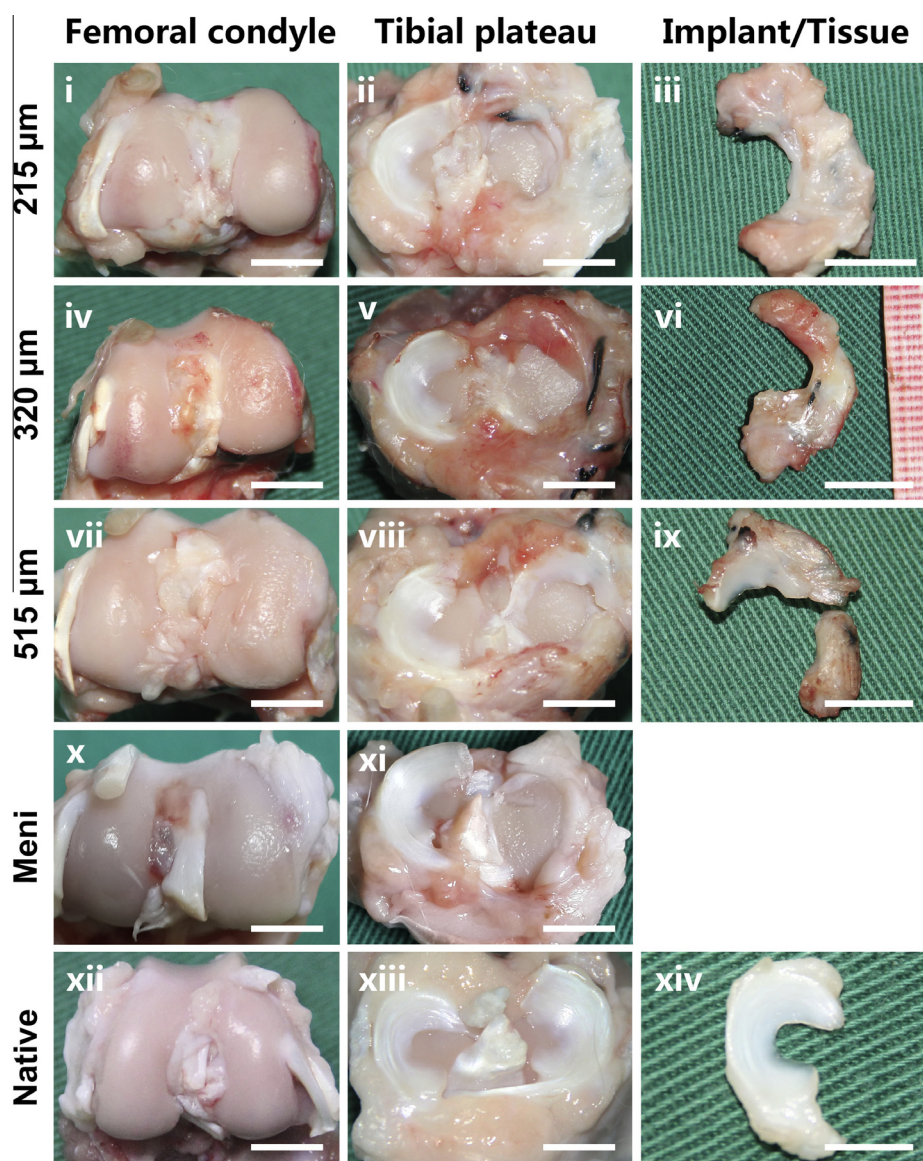

Fig. 4. Macroscopic observations of joints and implants at postoperative 12 weeks. Scale bar represented 10 mm.

response consisting of mononuclear cell infiltration with the residual scaffold was presented in almost all the implants, which was more evident in the hypocellularity area. More vascularization was detected in outer regions of the neomenisci (Fig. 6). For the 215 μm scaffold group, the scaffold was surrounded by peripheral synovial cells that incorporated into the pores of implant. Similar
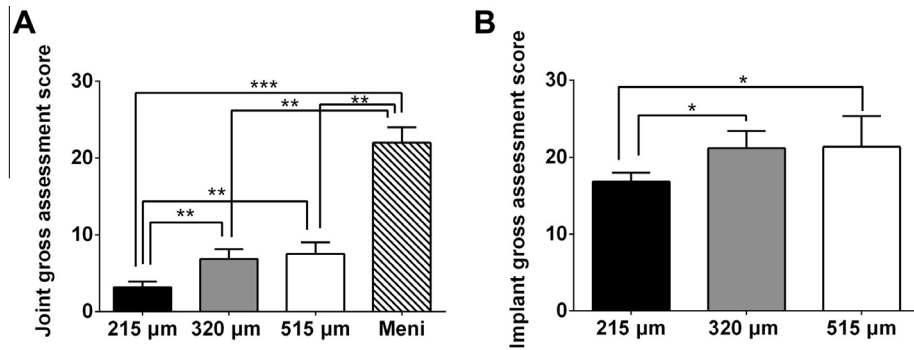
Fig. 5. Joint and implant gross assessment scores. Based on joint gross assessment score (A), a significantly lower joint degeneration was observed in the 215 μm scaffold group as compared to those of the other groups. In implant gross assessment score (B), better implant appearance was observed in the group of 215 μm scaffold. (n = 6; *P < 0.05, **P < 0.01, ***P < 0.001).
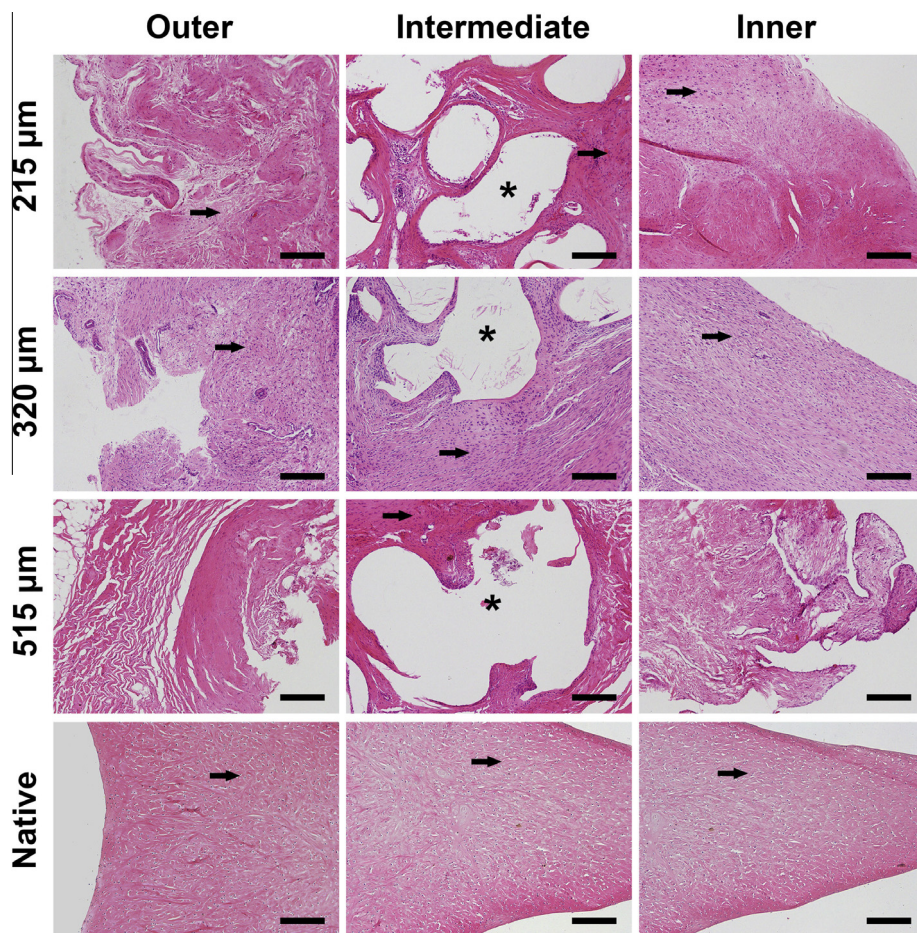

Fig. 6. Representative H&E microimages of regenerated and native menisci. Fibrochondrocyte-like cells marked by black arrows were observed in the implants at 12 weeks, especially in the 215 μm scaffold group. White void spaces (∗) represented the dissolved scaffolds. Scale bar represented 100 μm.

to native meniscus, the fibrocartilage differentiation was detected with fibrochondrocyte-like phenotype surrounded by ECM with abundant Col I and Col II antibody labeling and TB staining. In addition, more Col I was demonstrated in the 215 μm scaffold group by PSR staining. On the other hand, poor synovial cell infiltration and subsequent weak metachromatic staining of tissue were observed for the other groups (Figs. 7 and 8). According to the semiquantitative analysis of collagen content, the increasing matrix staining with Col I and Col II was more apparent in the 215 μm implant (P < 0.05; Fig. 9).

3.7. Evaluation of articular cartilage

In histological evaluation (Fig. 10), the femoral condyle and tibial plateau showed complete disorganization of the cartilage combination with severe reduction of TB staining in total meniscectomy (Meni) group. Although with less severe cartilage damage than that of the Meni group, the 320 or 525 μm scaffold groups revealed clefts to the transitional or radial zone and diffuse chondrocyte cloning with slight reduction of TB staining. Compared to the above groups, the situation of the 215 μm scaffold
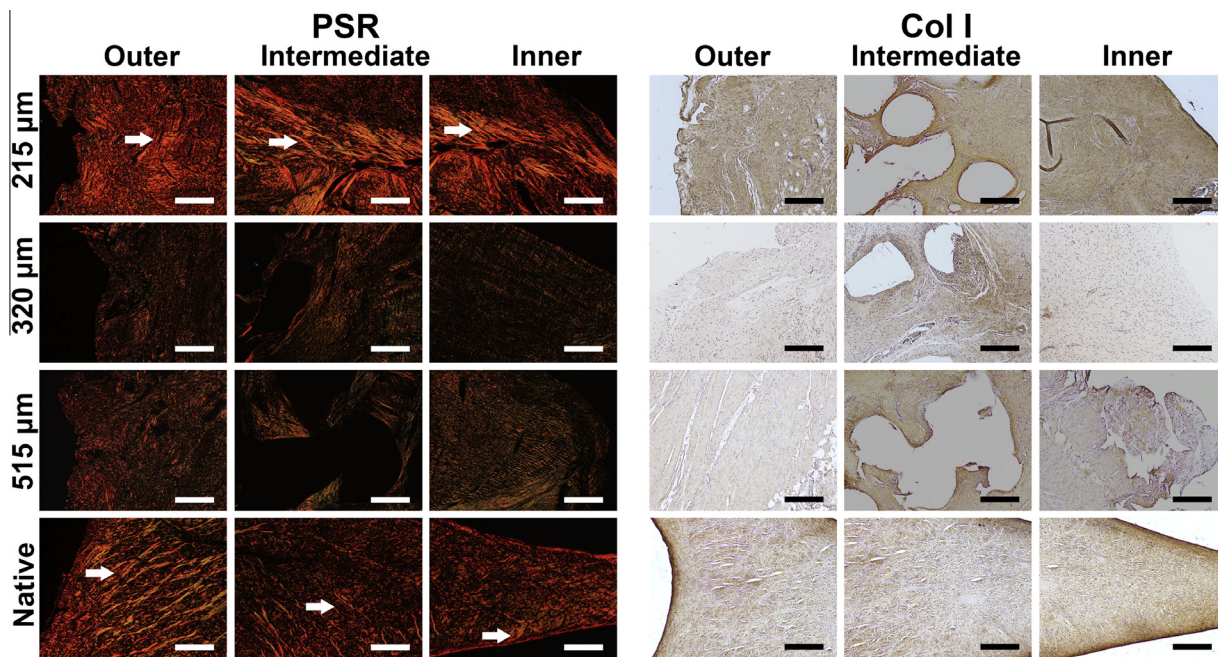
Fig. 7. Representative PSR and immunohistochemical staining for Col I of regenerated and native menisci. Crassi red fiber represented Col I noted by white arrows. Scale bar represented 100 µm. (For interpretation of the references to colour in this figure legend, the reader is referred to the web version of this article.)
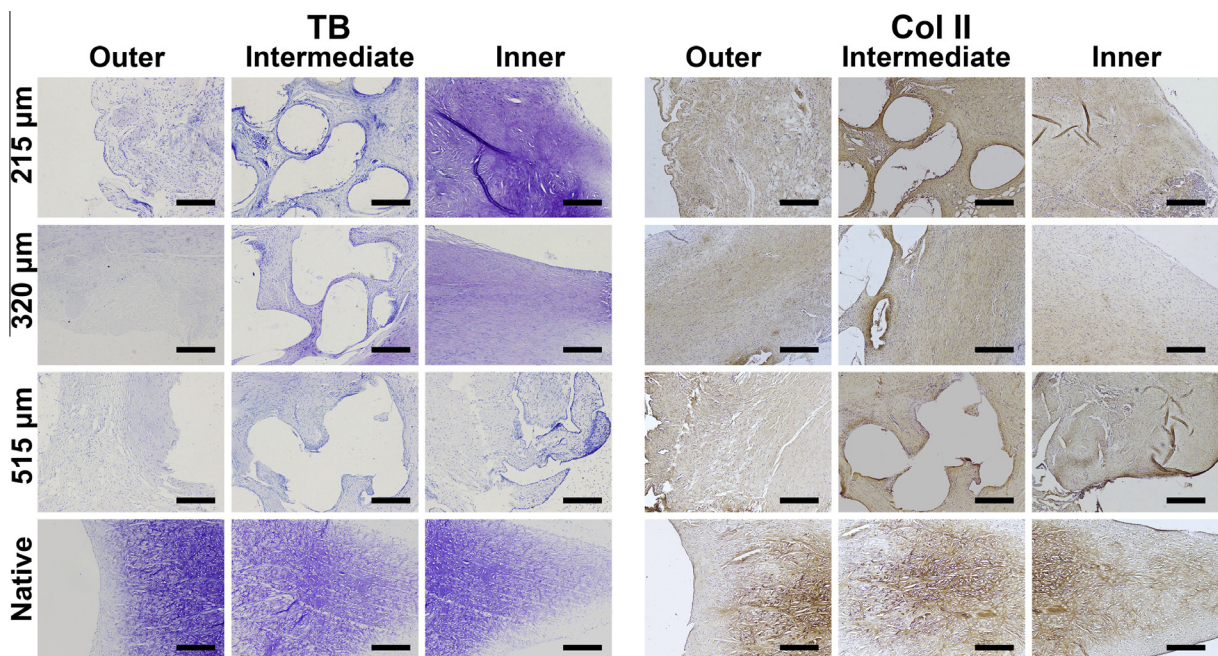

Fig. 8. Representative TB and immunohistochemical staining for Col II of regenerated and native menisci. Scale bar represented 100 µm.

group was significantly better and only pannus or surface irregularities with diffuse hypercellularity were displayed.

The ICRS and Mankin scores are shown in Fig. 11, and Supplementary Tables S5 and S7, and all of the joint cartilages were damaged, especially in medial tibial plateau. A relatively better chondroprotection was found with the 215 µm scaffold in both femur and tibia side ($P < 0.05$). However, there was no significant difference of the ICRS scores between the 320/515 µm scaffold group and the Meni group ($P > 0.05$), while the better results of 320/515 µm scaffold group were shown of the Mankin scores except for 515 µm scaffold group in tibial plateau.

4. Discussion

The overall goal of this study is to investigate the influences of various mean pore sizes of FDM-printed PCL scaffolds on meniscus regeneration. By altering FDM processing condition, the PCL scaffolds with three distinct mean pore sizes of 215, 325, and 515 µm possess decreasing specific surface areas. The results demonstrated the role of the mean pore size of PCL scaffold in the behaviors of endogenous or exogenous stem/progenitor cells, and subsequent tissue formation both *in vitro* and *in vivo*, thus highlighting the importance of scaffold
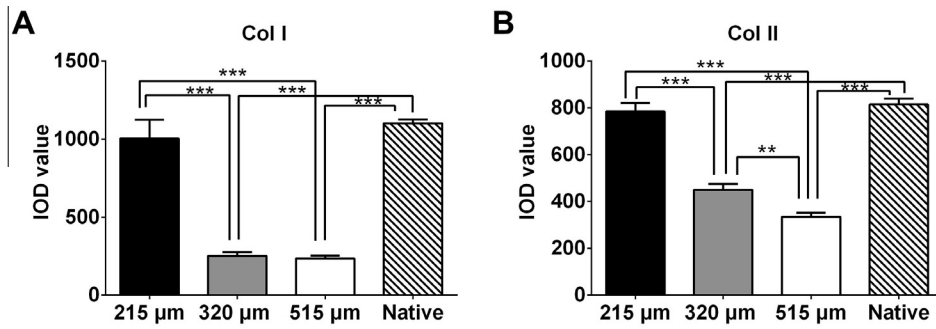
Fig. 9. Immunohistochemical analyses of native meniscus and implants. The largest integrated optical density (IOD) values of Col I (A) and Col II (B) were observed in the 215 μm implant group than the other implant ones, similar to the native meniscus ($n = 6$; $^{**}P < 0.01$, $^{***}P < 0.001$).
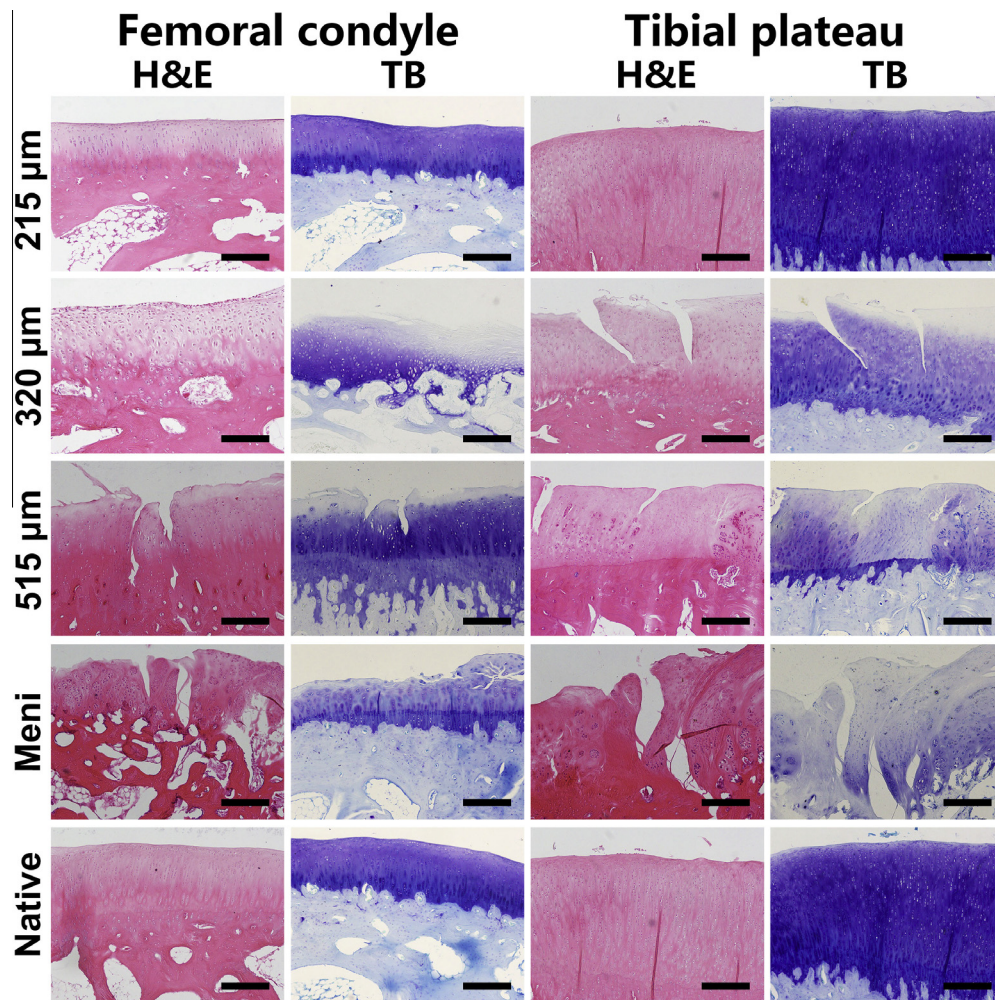

Fig. 10. H&E and TB staining of articular cartilage surfaces in femoral condyle and tibial plateau. Most insignificant joint degeneration was observed in the 215 μm scaffold group. Scale bar represented 100 μm.

architecture in the development of biomaterials for meniscus tissue engineering.

According to the results on the adhesion and proliferation of MSCs *in vitro*, the scaffold with the largest mean pore size had the significantly lowest number of cells than those with the relative smaller mean pore sizes of 215 and 325 μm. In spite of no difference between the latter two groups in initial cell attachment analyses, a strong linear relationship between SA/V and the area of MSC colonization was found for the first time (Fig. 2J).

Furthermore, the scaffold with the smallest mean pore size provides the largest area for cell colonization and subsequently the greatest proliferation, which may have potential downstream effect, such as differentiation and matrix deposition. The little differences of cell attachment and proliferation analyses between the two groups of 215 and 325 μm might be explained by the effect of the too small mean pore size on the nutrition diffusion and seed cell migration [32,33], which was shown in the LIVE/DEAD microimages and the percentage of live cells (Fig. S3B and S3C,
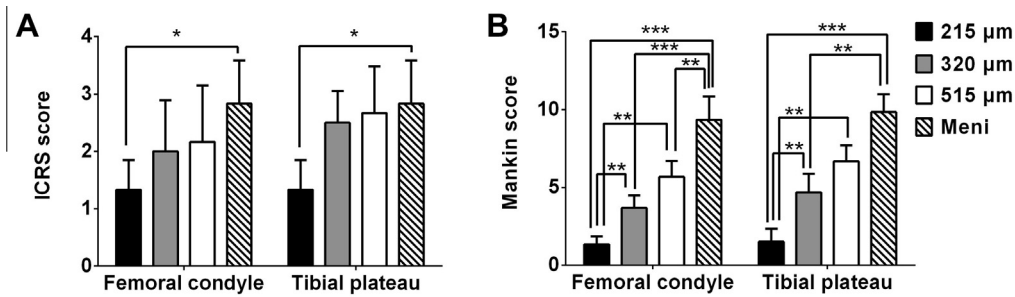
Fig. 11. ICRS and Mankin scores. The implantation of 215 μm scaffold provided the greatest chondroprotection in both femur and tibia based on ICRS (A) and Mankin scores (B) ($n = 6$; $^*P < 0.05$, $^{**}P < 0.01$, $^{***}P < 0.001$).

Supplementary data). As reported previously, larger interconnective pores (250–500 μm) in the scaffold could benefit effective nutrient supply and metabolic waste removal, while smaller pores (50–200 μm) did the opposite, resulting in inferior matrix productions [13]. Thus the 215 μm might be a favorable lower limit of the mean pore size of the scaffolds, and the pore sizes smaller than 215 μm would not be included in this research.

Another notable result from the study is that the mean pore size of scaffold would influence fibrochondrogenic differentiation and matrix production/deposition of MSCs both *in vitro* and *in vivo*. MSCs are promising cell source for meniscus tissue engineering due to its multipotent differentiation and immunoregulatory capacities [34]. By now, there has been still no acknowledged protocol for fibrocartilaginous differentiation of MSCs. The differentiation medium of MSCs used in the present study was previous described in other meniscus research [35], which might mainly induce chondrogenic differentiation of MSCs [36]. Although there was a relatively low level of Col I contrast to Col II in both gene and biochemical analyses after 2 weeks *in vitro* culture, higher AGC and Col II gene expression was stimulated in the 215 and 325 μm scaffolds than in the 515 μm scaffold. The potential reason is that the scaffolds with above microarchitectures possess sufficient areas for cell adhesion and proliferation, which may affect the subsequent cell differentiation and tissue formation. In addition, immunofluorescence staining of the cytoskeleton on the distinct scaffold variants reveals another interesting insight. It was known that the difference in cell behavior may be partly attributed to their shape and colonization [5,37]. In the present study, the smallest mean pore size scaffold with the greatest specific surface area facilitates 3D cell colonization and the bridge of neighboring fibers (Fig. 2D–F), which result in superior potential in differentiation. The positive correlation between SA/V and the area of Col II deposition indicated the role of mean pore size on tissue formation (Fig. 2K).

Theoretically, meniscal-derived fibrochondrocytes might be the optimal seeding cells for tissue engineering meniscus. However, dedifferentiation and senescence were detected with the time in our early research (data not shown), and the number of primary and passaged meniscus cells could not meet desired requirements. As widely used seeding cells in tissue engineering, MSCs have been confirmed to be with strong proliferation and multi-differentiation, and thus were utilized in the present study. By now, it is still a controversial issue about how to induce MSCs into fibrochondrocytes *in vitro*, thus MSCs in the present study were differentiated in the chondrogenic culture condition, thus inducing more Col II and GAG production which was far from the native meniscus histological structure. Furthermore, native meniscus is an anisotropic fibrocartilaginous tissue, in which Col I is dominantly distributed in the outer zone but both Col I and Col II plus GAG can be identified in the inner zone [34]. Thus the *in vitro* cultured cell-scaffold constructs of the present study seemed histologically closer to

hyaline cartilage or inner part of the native meniscus. However, it was interested that the fibrocartilaginous tissue formation was observed after 12 weeks implantation *in vivo*, especially in the 215 μm scaffold group (Fig. 7). In fact, all the reported inducing conditions *in vitro* by now had few effect on fibrocartilaginous formation compared to the *in vivo* results. The study focused on simulation of the *in vivo* biochemical and biomechanical microenvironments might be necessary to construct with ECM and biomechanics close to the native meniscus. In addition, further study is needed to investigate the effect of mean pore size on the other fibrocartilage-like cell differentiation protocol [38].

The scaffolds for tissue engineering should possess sufficient mechanical strength to withstand the stress generated by cells and load *in vivo*. As tissue-engineered meniscus plays a key role in joint load distribution similarly with the native meniscus, the requirement of biomechanical property should also be kept in mind especially for the case *in vivo*. Unfortunately, few scaffolds have been comparable to the tensile modulus of native meniscus up to now [38]. In this study, FDM were utilized to fabricate the PCL scaffold for regeneration of tissue-engineered meniscus. Firstly, compared with the other natural materials or synthetic polymers used in meniscus tissue engineering, PCL would be a promising material because of its superior mechanical characters, bioactivity, and processability [4,34]. Moreover, compared to the traditional processing methods, such as lyophilization [39] and electrospinning [35], FDM is a rapid prototyping technique that can produce 3D architectures with complete control of the geometrical parameters, such as pore size, porosity, and pore interconnection size [40], which have an effect on the mechanical properties of porous scaffolds [17]. In this study, both the acellular and cellular scaffolds with mean pore size of 215 μm exhibited the greatest tensile and compressive moduli in the three groups. There was indeed no significant difference of the tensile and compressive moduli of 215 μm scaffolds on day 0 and 28. In spite of the secretion of Col II and GAG by the seeded MSCs after cultivation, the increase of biomechanics *in vitro* was still difficult for the existing technique and might need much more cell, matrix, and time.

With stronger biomechanics than the other groups, the 215 μm scaffold might become more resistive to the tensile and compressive loads after implantation, which was confirmed by the results *in vivo*. As anticipated, the grafted 215 μm scaffold provided the greatest protection of articular cartilage in both femur and tibia. Although polymer fiber degradation may reduce the mechanical properties of implants, the tissue ingrowth and adequate ECM can compensate to maintain the mechanical strength [4]. More importantly, the fibrocartilaginous tissue formation was also significantly more frequent in the 215 μm construct. Thus the superiority of 215 μm scaffold in the chondroprotective effect might become more obvious with time. The scaffolds with larger pore sizes (*i.e.*, 515 μm) were damaged due to the mechanical weakness. In fact, this performance resulted from initial mechanical property

and following tissue ingrowth, which were closely related to pore size.

The present study is a primary exploration about the mean pore sizes of FDM-printed PCL scaffolds, which are rarely reported but might be a crucial factor for tissue engineering meniscus. However, different material scaffolds with diverse mean pore sizes should also been investigated in the future. The present results also indicated that FDM might provide a rapid and repeatable method to direct the formation of an anatomic meniscus construct with architecture-dependent properties for the partial or total replacement of the knee meniscus, which should be evaluated though a long-term study *in vivo*.

In contrast to cell transplantation, the present study reported the generation of a functional meniscus in a rabbit model with strategy of endogenous regeneration. Regeneration by cell homing is a one-step procedure, which provides a promising alternative to cell transplantation [6,41]. However, how the recruited endogenous cells (*i.e.*, stem/progenitor cells) interacted with scaffold in microenvironment has not been investigated completely [42]. The stem/progenitor cells for meniscus regeneration in the present study might be derived from synovium [43] or peripheral blood in the wound [18]. Furthermore, the age of animal model should also be taken into research consideration in this research. The juvenile rabbits were selected for its skeletal maturity with the joint matching of the implant. In addition, this age group might have less effect on the degradation of cartilage and risk of postoperative complications compared to older issues. The comparison of animal in different ages in one-step procedure might be needed in the future.

Furthermore, processing scaffold with smaller pore size requests more-refined road width and spacing, which exceed the threshold parameters. Only three distinct mean pore sizes (*i.e.*, 215, 320, and 515 μm) were evaluated, and the scaffolds with extending mean pore sizes will be further investigated. Moreover, the mechanical properties of scaffold were still inferior to those of native meniscus (75–150 MPa), the architecture of scaffold should be modified by the regulation of processing condition. Besides, the long-term *in vivo* evaluation is needed in the future in spite of the promising results after implantation for 12 weeks.

5. Conclusions

In this study, the mean pore size of 3D-printed PCL scaffold was confirmed to affect cell behavior, ECM production, biomechanics, and rehabilitation. The 3D-printed PCL scaffold with mean pore size of 215 μm demonstrated optimal cell behaviors, ECM production and deposition, and resultant mechanical properties both *in vitro* and *in vivo*, providing an alternative for meniscus tissue engineering. The results also further the understanding of the cell-scaffold interaction in the researches of meniscus tissue engineering, which provides deep insight into the design of meniscal scaffold in the future.

Acknowledgments

Appendix A. Supplementary data

Supplementary data associated with this article can be found, in the online version, at http://dx.doi.org/10.1016/j.actbio.2016.07.050.

References

[1] W.E. Garrett Jr., M.F. Swiontkowski, J.N. Weinstein, J. Callaghan, R.N. Rosier, D.J. Berry, J. Harrast, G.P. Derosa, American board of orthopaedic surgery practice of the orthopaedic surgeon: Part-II, certification examination case mix, J. Bone Joint Surg. Am. 88 (3) (2006) 660–667.

[2] J.N. Katz, R.H. Brophy, C.E. Chaisson, L. de Chaves, B.J. Cole, D.L. Dahm, L.A. Donnell-Fink, A. Guermazi, A.K. Haas, M.H. Jones, B.A. Levy, L.A. Mandl, S.D. Martin, R.G. Marx, A. Miniaci, M.J. Matava, J. Palmisano, E.K. Reinke, B.E. Richardson, B.N. Rome, C.E. Safran-Norton, D.J. Skonieci, D.H. Solomon, M.V. Smith, K.P. Spindler, M.J. Stuart, J. Wright, R.W. Wright, E. Losina, Surgery versus physical therapy for a meniscal tear and osteoarthritis, N. Engl. J. Med. 368 (18) (2013) 1675–1684.

[3] P.U. Brucker, A. von Campe, D.C. Meyer, D. Arbab, L. Stanek, P.P. Koch, Clinical and radiological results 21 years following successful, isolated, open meniscal repair in stable knee joints, Knee 18 (6) (2011) 396–401.

[4] Z.Z. Zhang, D. Jiang, S.J. Wang, Y.S. Qi, J.X. Ding, J.K. Yu, X.S. Chen, Scaffolds drive meniscus tissue engineering, RSC Adv. 5 (95) (2015) 77851–77859.

[5] G. Kumar, C.K. Tison, K. Chatterjee, P.S. Pine, J.H. McDaniel, M.L. Salit, M.F. Young, C.G. Simon Jr., The determination of stem cell fate by 3D scaffold structures through the control of cell shape, Biomaterials 32 (35) (2011) 9188–9196.

[6] A.T. Neffe, B.F. Pierce, G. Tronci, N. Ma, E. Pittermann, T. Gebauer, O. Frank, M. Schossig, X. Xu, B.M. Willie, M. Forner, A. Ellinghaus, J. Lienau, G.N. Duda, One step creation of multifunctional 3D architectured hydrogels inducing bone regeneration, Adv. Mater. 27 (10) (2015) 1738–1744.

[7] A. Matsiko, J.P. Gleeson, F.J. O'Brien, Scaffold mean pore size influences mesenchymal stem cell chondrogenic differentiation and matrix deposition, Tissue Eng. Part A 21 (3–4) (2015) 486–497.

[8] S. Ryu, J. Yoo, Y. Jang, J. Han, S.J. Yu, J. Park, S.Y. Jung, K.H. Ahn, S.G. Im, K. Char, B.S. Kim, Nanothin coculture membranes with tunable pore architecture and thermoresponsive functionality for transfer-printable stem cell-derived cardiac sheets, ACS Nano 9 (10) (2015) 10186–10202.

[9] F.J. O'Brien, B.A. Harley, I.V. Yannas, L.J. Gibson, The effect of pore size on cell adhesion in collagen-GAG scaffolds, Biomaterials 26 (4) (2005) 433–441.

[10] L.P. Yan, J.M. Oliveira, A.L. Oliveira, S.G. Caridade, J.F. Mano, R.L. Reis, Macro/microporous silk fibroin scaffolds with potential for articular cartilage and meniscus tissue engineering applications, Acta Biomater. 8 (1) (2012) 289–301.

[11] B.B. Mandal, S.H. Park, E.S. Gil, D.L. Kaplan, Multilayered silk scaffolds for meniscus tissue engineering, Biomaterials 32 (2) (2011) 639–651.

[12] B.D. Smith, D.A. Grande, The current state of scaffolds for musculoskeletal regenerative applications, Nat. Rev. Rheumatol. 11 (4) (2015) 213–222.

[13] S.M. Lien, L.Y. Ko, T.J. Huang, Effect of pore size on ECM secretion and cell growth in gelatin scaffold for articular cartilage tissue engineering, Acta Biomater. 5 (2) (2009) 670–679.

[14] J. Klompmaker, H.W. Jansen, R.P. Veth, H.K. Nielsen, J.H. de Groot, A.J. Pennings, Porous implants for knee joint meniscus reconstruction: a preliminary study on the role of pore sizes in ingrowth and differentiation of fibrocartilage, Clin. Mater. 14 (1) (1993) 1–11.

[15] N. Xu, X. Ye, D. Wei, J. Zhong, Y. Chen, G. Xu, D. He, 3D artificial bones for bone repair prepared by computed tomography-guided fused deposition modeling for bone repair, ACS Appl. Mater. Interfaces 6 (17) (2014) 14952–14963.

[16] Z. Man, L. Yin, Z. Shao, X. Zhang, X. Hu, J. Zhu, L. Dai, H. Huang, L. Yuan, C. Zhou, H. Chen, Y. Ao, The effects of co-delivery of BMSC-affinity peptide and rhTGF-beta1 from coaxial electrospun scaffolds on chondrogenic differentiation, Biomaterials 35 (19) (2014) 5250–5260.

[17] I. Zein, D.W. Hutmacher, K.C. Tan, S.H. Teoh, Fused deposition modeling of novel scaffold architectures for tissue engineering applications, Biomaterials 23 (4) (2002) 1169–1185.

[18] W.L. Fu, C.Y. Zhou, J.K. Yu, A new source of mesenchymal stem cells for articular cartilage repair: MSCs derived from mobilized peripheral blood share similar biological characteristics *in vitro* and chondrogenesis *in vivo* as MSCs from bone marrow in a rabbit model, Am. J. Sports Med. 42 (3) (2014) 592–601.

[19] Z.Z. Zhang, D. Jiang, S.J. Wang, Y.S. Qi, J.Y. Zhang, J.K. Yu, Potential of centrifugal seeding method in improving cells distribution and proliferation on demineralized cancellous bone scaffolds for tissue-engineered meniscus, ACS Appl. Mater. Interfaces 7 (28) (2015) 15294–15302.

[20] R.W. Farndale, D.J. Buttle, A.J. Barrett, Improved quantitation and discrimination of sulphated glycosaminoglycans by use of dimethylmethylene blue, Biochim. Biophys. Acta 883 (2) (1986) 173–177.

[21] D.J. Huey, K.A. Athanasiou, Tension-compression loading with chemical stimulation results in additive increases to functional properties of anatomic meniscal constructs, PLoS ONE 6 (11) (2011) e27857.

[22] P. Li, X. Feng, X. Jia, Y. Fan, Influences of tensile load on *in vitro* degradation of an electrospun poly(L-lactide-*co*-glycolide) scaffold, Acta Biomater. 6 (8) (2010) 2991–2996.

[23] C.S. Proctor, M.B. Schmidt, R.R. Whipple, M.A. Kelly, V.C. Mow, Material properties of the normal medial bovine meniscus, J. Orthop. Res. 7 (6) (1989) 771–782.

[24] C. Liu, R. Abedian, R. Meister, C. Haasper, C. Hurschler, C. Krettek, G. von Lewinski, M. Jagodzinski, Influence of perfusion and compression on the proliferation and differentiation of bone mesenchymal stromal cells seeded on polyurethane scaffolds, Biomaterials 33 (4) (2012) 1052–1064.

[25] J.L. Drury, R.G. Dennis, D.J. Mooney, The tensile properties of alginate hydrogels, Biomaterials 25 (16) (2004) 3187–3199.

[26] D. Jiang, L.H. Zhao, M. Tian, J.Y. Zhang, J.K. Yu, Meniscus transplantation using treated xenogeneic meniscal tissue: viability and chondroprotection study in rabbits, Arthroscopy 28 (8) (2012) 1147–1159.

[27] D.W. Jackson, C.A. McDevitt, T.M. Simon, S.P. Arnoczky, E.A. Atwell, N.J. Silvino, Meniscal transplantation using fresh and cryopreserved allografts: an experimental study in goats, Am. J. Sports Med. 20 (6) (1992) 644–656.

[28] E. Kon, C. Chiari, M. Marcacci, M. Delcogliano, D.M. Salter, I. Martin, L. Ambrosio, M. Fini, M. Tschon, E. Tognana, R. Plasenzotti, S. Nehrer, Tissue engineering for total meniscal substitution: animal study in sheep model, Tissue Eng. Part A 14 (6) (2008) 1067–1080.

[29] M. Brittberg, C.S. Winalski, L. Lippiello, Evaluation of cartilage injuries and repair, J. Bone Joint Surg. Am. 85-A (Suppl. 2) (2003) 58–69.

[30] H.J. Mankin, H. Dorfman, L. Lippiello, A. Zarins, Biochemical and metabolic abnormalities in articular cartilage from osteo-arthritic human hips. II. Correlation of morphology with biochemical and metabolic data, J. Bone Joint Surg. Am. 53 (3) (1971) 523–537.

[31] S. Miot, T. Woodfield, A.U. Daniels, R. Suetterlin, I. Peterschmitt, M. Heberer, C. A. van Blitterswijk, J. Riesle, I. Martin, Effects of scaffold composition and architecture on human nasal chondrocyte redifferentiation and cartilaginous matrix deposition, Biomaterials 26 (15) (2005) 2479–2489.

[32] D.J. Griffon, M.R. Sedighi, D.V. Schaeffer, J.A. Eurell, A.L. Johnson, Chitosan scaffolds: interconnective pore size and cartilage engineering, Acta Biomater. 2 (3) (2006) 313–320.

[33] S.H. Oh, I.K. Park, J.M. Kim, J.H. Lee, In vitro and in vivo characteristics of PCL scaffolds with pore size gradient fabricated by a centrifugation method, Biomaterials 28 (9) (2007) 1664–1671.

[34] E.A. Makris, P. Hadidi, K.A. Athanasiou, The knee meniscus: structure-function, pathophysiology, current repair techniques, and prospects for regeneration, Biomaterials 32 (30) (2011) 7411–7431.

[35] B.M. Baker, R.L. Mauck, The effect of nanofiber alignment on the maturation of engineered meniscus constructs, Biomaterials 28 (11) (2007) 1967–1977.

[36] R.L. Mauck, X. Yuan, R.S. Tuan, Chondrogenic differentiation and functional maturation of bovine mesenchymal stem cells in long-term agarose culture, Osteoarthr. Cartil. 14 (2) (2006) 179–189.

[37] G.M. Harris, M.E. Piroli, E. Jabbarzadeh, Deconstructing the effects of matrix elasticity and geometry in mesenchymal stem cell lineage commitment, Adv. Funct. Mater. 24 (16) (2014) 2396–2403.

[38] C.H. Lee, S.A. Rodeo, L.A. Fortier, C. Lu, C. Erisken, J.J. Mao, Protein-releasing polymeric scaffolds induce fibrochondrocytic differentiation of endogenous cells for knee meniscus regeneration in sheep, Sci. Transl. Med. 6 (266) (2014) 266ra171.

[39] C. Yu, J. Bianco, C. Brown, L. Fuetterer, J.F. Watkins, A. Samani, L.E. Flynn, Porous decellularized adipose tissue foams for soft tissue regeneration, Biomaterials 34 (13) (2013) 3290–3302.

[40] A.D. Lantada, P.L. Morgado, Rapid prototyping for biomedical engineering: current capabilities and challenges, Annu. Rev. Biomed. Eng. 14 (2012) 73–96.

[41] H. Huang, X. Zhang, X. Hu, Z. Shao, J. Zhu, L. Dai, Z. Man, L. Yuan, H. Chen, C. Zhou, Y. Ao, A functional biphasic biomaterial homing mesenchymal stem cells for in vivo cartilage regeneration, Biomaterials 35 (36) (2014) 9608–9619.

[42] C.H. Lee, J.L. Cook, A. Mendelson, E.K. Moioli, H. Yao, J.J. Mao, Regeneration of the articular surface of the rabbit synovial joint by cell homing: a proof of concept study, Lancet 376 (9739) (2010) 440–448.

[43] C. De Bari, F. Dell'Accio, P. Tylzanowski, F.P. Luyten, Multipotent mesenchymal stem cells from adult human synovial membrane, Arthritis Rheum. 44 (8) (2001) 1928–1942.